



저작자표시-비영리-변경금지 2.0 대한민국

이용자는 아래의 조건을 따르는 경우에 한하여 자유롭게

- 이 저작물을 복제, 배포, 전송, 전시, 공연 및 방송할 수 있습니다.

다음과 같은 조건을 따라야 합니다:



저작자표시. 귀하는 원저작자를 표시하여야 합니다.



비영리. 귀하는 이 저작물을 영리 목적으로 이용할 수 없습니다.



변경금지. 귀하는 이 저작물을 개작, 변형 또는 가공할 수 없습니다.

- 귀하는, 이 저작물의 재이용이나 배포의 경우, 이 저작물에 적용된 이용허락조건을 명확하게 나타내어야 합니다.
- 저작권자로부터 별도의 허가를 받으면 이러한 조건들은 적용되지 않습니다.

저작권법에 따른 이용자의 권리는 위의 내용에 의하여 영향을 받지 않습니다.

이것은 [이용허락규약\(Legal Code\)](#)을 이해하기 쉽게 요약한 것입니다.

[Disclaimer](#)

Master's Thesis

Microstructural Change of Graphene Oxide Liquid Crystals with Polymer Crystallization

Soh Jin Mun

Department of Chemical Engineering

Graduate School of UNIST

2019

**Microstructural Change of Graphene Oxide
Liquid Crystals with Polymer Crystallization**

Soh Jin Mun

Department of Chemical Engineering

Graduate School of UNIST

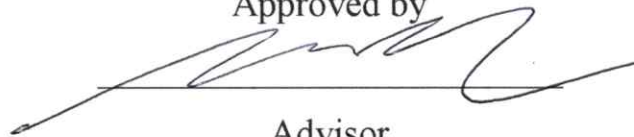
Microstructural Change of Graphene Oxide Liquid Crystals with Polymer Crystallization

A thesis/dissertation
submitted to the Graduate School of UNIST
in partial fulfillment of the
requirements for the degree of
Master of Science

Soh Jin Mun

06.18.2019

Approved by



Advisor

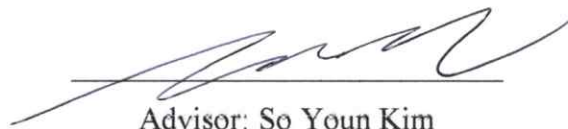
So Youn Kim

Microstructural Change of Graphene Oxide Liquid Crystals with Polymer Crystallization

Soh Jin Mun

This certifies that the thesis/dissertation of Soh Jin Mun is approved.

06. 18. 2019 of submission



Advisor: So Youn Kim



Joonwoo Jeong



Dong-Woog Lee

Abstract

Graphene Oxides (GO) have been frequently employed as fillers in polymer based applications. In GO-polymer composites, GO is known to nucleate polymer crystallizations, reinforcing mechanical property of semicrystalline polymers. In this regard, many prior studies investigated GO-induced polymer crystallization. However, the counter effect that how polymer crystallization can change the microstructure of GO was not seriously considered thus, has not been systemically studied yet. As GO can form nematic liquid crystal (LC) phase in aqueous solution, GO LC and polymer crystals co-exist in GO/PEG complex where the overall GO LC is dramatically decreased by the polymer crystallization. To find a correlation between the GO LC and polymer crystallization, we change the cooling rate in polymer crystallization process. While polymer crystallizes in bulk or at interface depending on the cooling rate, an interfacial crystallization of poly(ethylene glycol) (PEG) on the GO improved both GO alignment and orientation of PEG crystal. This work provides an opportunity to develop a hierarchical structure of GO-based crystalline polymer nanocomposites whose directionality can be controlled by polymer crystallization with proper cooling rates.

Contents

List of Figures -----	1
I. Introduction -----	2
1.1. Graphene -----	2
1.1.1. Definition and Property of Graphene	
1.2. Graphene Oxide Liquid Crystals -----	3
1.2.1. Definition and Property of Graphene Oxide	
1.2.2. Discovery of Graphene Oxide Liquid Crystal	
1.2.3. Characterization of Nematic Phase Formation of Graphene Oxide Liquid Crystal	
1.3 Graphene Oxide Liquid Crystals with Polymer Crystallization -----	5
1.3.1. Graphene-Polymer Nanocomposite	
1.3.2. Graphene Oxide Liquid Crystal Under Controlled Crystalline Circumstance	
II. Experimental Method & Materials-----	7
2.1. Sample Preparation	
2.2. Cooling rate controls for polymer crystallization	
2.3. Polarized Optical Microscopy (POM)	
2.4. Differential Scanning Calorimetry (DSC)	
2.5. Synchrotron X-ray Characterization	
2.6. Preparation of GO/PEG Film	

III. Results and Discussion-----	9
3.1. GO LC behavior in bulk system-----	9
3.1.1. GO LC behavior with polymer crystallization	
3.1.2. Polymer Crystallization with GO LC at Controlled Cooling Rate	
3.1.3 Effect of Cooling Rate on GO LC with Polymer Crystallization	
3.1.4 Lamellar Thickness of PEG and d-spacing of GO at Different Cooling Rate	
3.2. GO LC behavior in film system -----	20
IV. Conclusion -----	23
4.1. GO LC behavior in bulk system	
4.2. GO LC behavior in film system	
References	

List of figures

Figure 1. Graphene and its different dimensional relatives

Figure 2. Structure of Graphene Oxide

Figure 3. Schematic image of temperature profiles to control the polymer crystallization

Figure 4. POM images of GO LC with the polymer crystallization

Figure 5. Selected 2D SAXS pattern of GP03 (a) and (b), GP15 (c) and (d) at different cooling rate

Figure 6. Development of WAXS profiles as a function of crystallization time for PEG (a) and GP15(b)

Figure 7. Kratky plots of GP03-fast (a) and slow (b), GP15-fast (c) and slow (d), and intensity of q^* versus time of GP03 (e)

Figure 8. Angle distribution curves at GP03-fast (a) and slow (b), GP15-fast (c) and slow (d)

Figure 9. HOF values as a function of crystallization time

Figure 10. The value of q^* from crystal lamellae as a function of time of GP03 (a) and GP15 (b), and long period calculated at final stage (c)

Figure 11. 1D plots of GP15-fast (a) and slow (b), and d-spacing of GO in GP15 (c)

Figure 12. Schematic images of GO LC with polymer crystal structure cooling at fast and slow speed

Figure 13. Real image of GO/PEG film cooling at fast and slow speed

Figure 14. SEM images of cross-section of GP15-fast (a) and slow (b) film and the inset image show SAXS 2D patterns of films

Figure 15. POM images of GO LC with PEG

I. Introduction

1.1. Graphene

1.1.1. Definition and Property of Graphene

Graphene is a single atomic plane of graphite, constructed with sp²-bonded carbon atoms in a perfect hexagonal lattice.¹ The π -conjugation of graphene in long-range enables extraordinary mechanical, thermal, and electrical properties, which have been the research interest of many theoretical studies and more recently became an exciting area for researchers.²

While studies of graphite have been focused on utilizing fewer and fewer layers for several time, Geim and co-workers first did successfully manufacturing isolated single-layer samples from graphite. This led to an explosion of interest and researches of lamellar solids to a new functional 2D nanomaterials.

¹ As the first freestanding 2D crystals, graphene begins to show promising potentials in wide range of application, such as flexible transparent electrodes, photoelectronics, multifunctional composites and new graphitic macroscopic materials.^{1, 3-4} Importantly, the interest on graphene materials provides a fundamentally fresh perspective in lamellar solid phase and guides the construction of the rich system of 2D nanomaterials.⁵⁻⁶ In addition to great hopes for future electronics, graphene and other 2D counterparts can be considered as 2D building blocks to construct macroscopic materials at atomic precision.

Generally, graphene could be considered as a basic building block of other graphitic materials, such as fullerenes, carbon nanotubes (CNTs) and graphite (**Figure1**). Graphene is a 2D building material for graphitic carbon materials of 0D buckyballs, 1D carbon nanotubes and 3D graphite.⁷

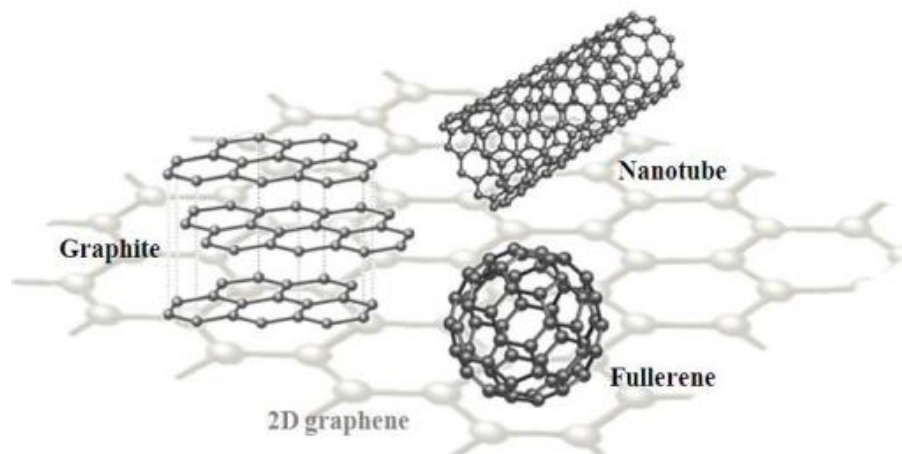


Figure 1. Graphene and its different dimensional relatives ⁸

1.2. Graphene Oxide Liquid Crystals

1.2.1. Emergence of Graphene Oxide

Graphene oxide (GO) is oxidized form of monolayer graphene platelet with strong mechanical properties, extremely large surface area, and chemical functionalization capability. Unlike pristine graphene, GO is decorated with dense covalently bonded oxygen functional groups such as carboxyl (COOH), hydroxyl (OH) and epoxide (ring COC) groups.⁹⁻¹¹ Although pristine graphene is preferred than GO for nanoelectronics applications, some degree of chemical functionalization could be required to be easy solution processing in many other applications. Herein, GO appears one of the most important precursor of graphene since exfoliated GO sheets can form stable aqueous dispersions in polar organic solvents including water. GO dispersion was highly desirable owing to the electrostatic repulsion among the deprotonated functional groups, such as carboxylates. Hence, GO was widely employed to prepare macroscopic papers,¹² polymer-based nanocomposites,¹³⁻¹⁶ inorganic nanoparticle – graphene hybrids.¹⁷⁻²¹ Likewise, GO has been an interesting material in its own right.

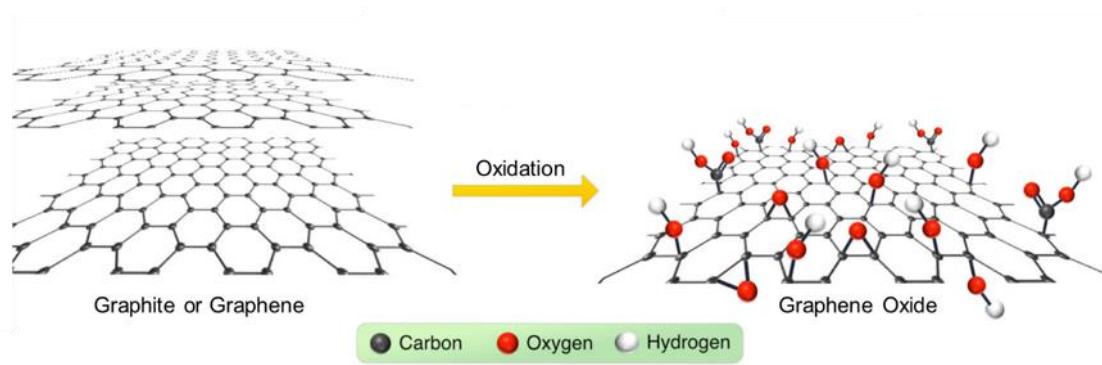


Figure 2. Structure of Graphene Oxide²²

1.2.2. Discovery of Graphene Oxide Liquid Crystal

One of the most noteworthy recent discovery was the presence of graphene oxide liquid crystals (GO LC). Liquid crystal (LC) is the ordered state of anisotropic particles that exhibit liquid-like fluidity but also demonstrate crystal-like ordering.²³ Along with the recent enormous interest in carbon materials, GO liquid crystals hold great promise for high-performance carbon material synthesis or device operation. Thus, graphene oxide liquid crystals (GO LC) were introduced as a new class of carbon-based liquid crystals.⁹

Because of its good solubility and the high aspect ratio, GO colloids form LCs in polar solvents including water. Benefiting from the ordering of GO LCs, GO was employed in the form of high performance fibers²⁴ and films²⁵. The stability of aqueous GO LC is mainly contributed to its hydrophilicity and electrostatic repulsions from negative-charged carboxylate groups.

1.2.3. Characterization of Nematic Phase Formation of Graphene Oxide Liquid Crystal

Generally, the structural information of LC fluid can be obtained with the measurements of polarized optical microscopy (POM) and small-angle X-ray scattering (SAXS). When GO dispersion is located between a pair of crossed polarizer, the GO sheet is oriented parallel to one of the crossed polarizer axes in the dark brushes but oriented in an intermediate direction in the bright brushes. Thus, GO LC show a strong birefringent Schlieren texture with bright and dark brushes in POM measurement. Xu and Gao confirmed the formation of nematic GO LC phase in aqueous solution through SAXS measurement.²⁶ In this study, the corresponding 2D patterns for GO LC dispersions exhibited an elliptical pattern with a larger axial ratio, indicating the increasing degree of orientation in the GO LCs. It could be originated from higher order lamellar phase at high concentration of GO sheets.

1.3. Graphene Oxide Liquid Crystals with Polymer Crystallization

1.3.1. Graphene-Polymer Nanocomposite

Graphene Oxide (GO) has brought tremendous attention in carbon-based nanocomposites as a promising materials due to its extraordinary mechanical, electrical, and thermal properties.^{9, 27-28} GO can be easily dispersed in polar solvents, thus GO becomes more preferential additives than other carbon materials added to nanocomposites. One of the most attractive applications of GO is GO based polymer nanocomposites where GOs are employed as an effective nanofiller especially in semicrystalline polymer matrix. In this application, GO exhibits a strong nucleating ability in various semicrystalline polymer promoting polymer crystallization in kinetics. The two-dimensional planar structure and high specific surface area of GO are believed to help the crystallization.²⁹ Previous researches showed that GO with high aspect ratio could induce intrachain ordering of isotactic polypropylene (iPP) at the surface, resulting in considerable elevation of overall crystallization rate of polymer.²⁹⁻³⁰

1.3.2. Graphene Oxide Liquid Crystal Under Controlled Crystalline Circumstance

Likewise, polymer crystallization may lead to the microstructural change of GOs. However, there is a lack of understanding how polymer crystallization can change the structure of the GOs in polymer solution. GO can also exhibit interesting nematic liquid crystallinity (LC) in aqueous solution, and its anisotropic property thereby enables highly ordered graphene-based fibers and films.³¹⁻³² In these application, polymer additives have been frequently employed to improve the physical properties of GO based materials. Thus, it is important to investigate the microstructural change of GO LC in polymer solution.

In this study, the change of GO LC in dense semicrystalline polymer solution is investigated. We hypothesize that the GO remains as liquid crystal (LC) phase in dense semicrystalline solution and the degree of liquid crystallinity is also changed by the degree and the type of polymer crystallization. We aim to understand the GO LC in the presence of polymer crystallization in a more systematic way for more advanced GO applications in nanocomposites.

GO nanosheets in polymer composites can be crumpled and aggregated when polymer crystallization occurs, resulting in the dramatically decreased LC/alignment of GO. Here, we show the degree of GO LC/alignment can be systematically controlled by the cooling rate for polymer crystallization. The fast cooling rate causes polymers to crystallize randomly in bulk, and the slow cooling rate causes them to preferentially crystallize on the surface of GO. Thus, the polymer crystallization proceeds in different ways depending on the cooling rate, dramatically changing the GO LC as a result.

Moreover, the effect of polymer crystallization on GO LC was also concentration dependent. As the GO concentration increases, the crystallization of polymers can be restricted because of the reduced

interspacing between GOs. Therefore, the change of GO LC with polymer crystallization is investigated by varying GO concentration and the cooling rate for polymer crystallization.

In this study, the correlation between the structure of GO LC and polymer crystals was investigated under the controlled polymer crystallization. Depending on the cooling rate for crystallization, the kinetics of polymer crystallization and the structure of polymer crystals change the GO LC. Small-angle X-ray scattering (SAXS) and polarized optical microscopy (POM) are employed to examine the microstructure of GO LC. In addition, the polymer crystal structure and the crystallinity are investigated through wide-angle X-ray Scattering (WAXS) and differential scanning calorimetry (DSC) experiment, respectively.

II. Experimental Method & Materials

2.1. Sample Preparation

The model system employed in this work is composed of aqueous GO suspensions and low molecular weight poly(ethylene glycol) (PEG). The polymer was purchased from Sigma-Aldrich ($M_n = 3350$ g/mol). GO was first suspended in water at 1 wt% after purifications as described elsewhere³³⁻³⁴, and then PEG solution, prepared at 20 wt%, was added to GO suspension. The GO/PEG complexes were left for 6 hours for stabilization, and then annealed under vacuum at 70 °C to dry/evaporate the water for the required time to reach the desired composition. Finally, the mixture of GO/crystallizable polymer complexes were prepared and the final concentration of GO was 0.3 and 1.5 wt% in PEG 80 wt%.

2.2. Cooling rate controls for polymer crystallization

Linkam TS1500 stage was set-up and used with a capillary cell for X-ray scattering studies to control the thermal history of the GO/PEG complexes. The exact experimental temperature profile was shown in Figure 1: i) initial heating at 10 °C/min rate from room temperature to 90 °C to remove the thermal history of GO/PEG complexes; ii) holding at 90 °C for 15 min; iii) cooling to 30 °C at a rate of 10 or 1 °C/min; iv) holding at 30 °C up to 24 hrs for polymer crystallization. The 10 or 1 °C/min was chosen for fast or slow cooling rate, respectively. The same temperature profiles given in **Figure 3** was employed for all experiments of SAXS, WAXS, POM and DSC.

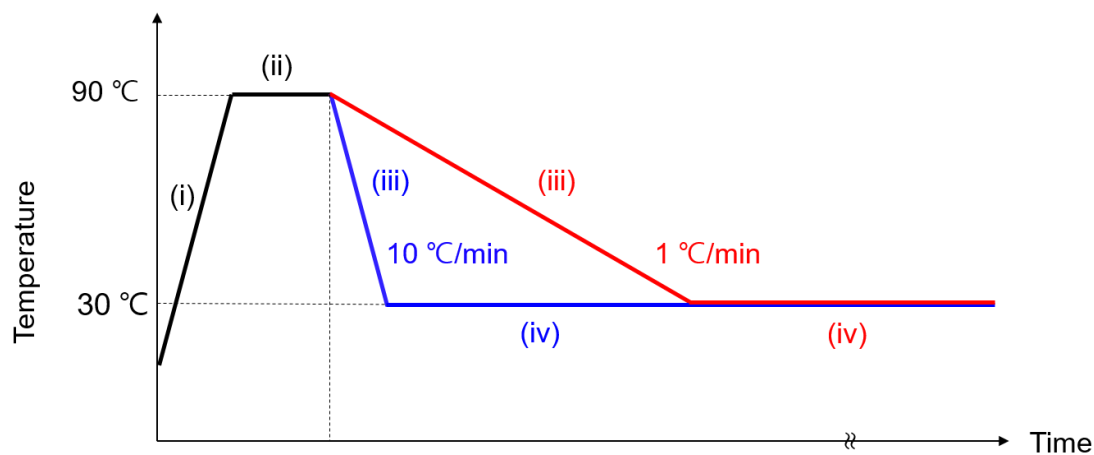


Figure 3. Schematic image of temperature profiles to control the polymer crystallization

2.3. Polarized Optical Microscopy (POM)

The LC phase of GO suspension in dense polymer solution was investigated by POM. The sample was slowly injected into a 1 mm thick glass cell, and images were taken at 50X magnification between two crossed polarizers using Olympus BX51 M microscope. To control the temperature conditions, a Linkam CSS-450 temperature stage was used equipped to the microscope.

2.4. Differential Scanning Calorimetry (DSC)

The DSC measurement was carried out using a differential scanning calorimeter (TA DSC Q2000). First, the samples of 5 to 10 mg were controlled through the temperature profiles in Figure 1 and the holding time at the step iv. is recorded. Then, the samples with different holding times were heated at a rate of 10 °C/min to 90 °C to calculate the degree of crystallinity of PEG in GO/PEG complexes.

2.5. Synchrotron X-ray Characterization

WAXS and SAXS experiments were conducted at the 6D and 9A Beamline of Pohang Accelerator Laboratory (PAL), respectively. For sample preparation, 200 µl of GO/PEG complex was injected at constant rate (3 ml/s) into a 1.5mm thick quartz capillary cell.

WAXS experiment provides the information about crystallization behavior of polymer at atomic scales. The sample-to-detector distance was 475 mm, and the X-ray energy was 18.986 keV. The scattered X-rays were analyzed with a CCD area detector (MX-225HS, Rayonix LLC). The 2D patterns were azimuthally integrated to a 1D profile of intensity versus scattering vector, $q = (4\pi \sin \theta)/\lambda$ (2θ is the scattering angle, and λ is the wavelength of X-ray).

To investigate microstructure of GO LC with polymer crystals, we performed SAXS experiment. The sample-to-detector distance was 4605 mm, and the X-ray energy was 11.045 keV. The scattered X-rays were analyzed with a CCD area detector (Rayonix SX165, USA).

2.6. Preparation of GO/PEG Film

GO/PEG films were prepared by the convenient blade-casting method. For the first time, the GO/PEG solution consisting of GO 0.3 wt% or 1.5 wt% and PEG 60 wt% were dropped on a mica substrate at 90 °C. After the blade casts the films at a speed of 5 mm s⁻¹, each film was cooled down at a speed of 10 and 1 °C/min. Finally, the films were dried at 30 °C under vacuum for overnight.

III. Results and Discussion

3.1. GO LC behavior in bulk system

3.1.1. GO LC behavior with polymer crystallization

The GO LC structure with polymer crystals was investigated through the POM measurement. The complex microstructure of GO LCs and polymer crystals were shown; the birefringes were partially shown and spherulites indicate formed polymer crystal structure (**Figure 4**). As polymer crystallization proceeds further, the increasingly dark brightness of GO LC was shown, which means the GO sheets lose its directionality by the growth of polymer crystals. While the observation with the POM confirms the existence of GO LC, the different behavior of GO LC between two cooling rates were unclear.

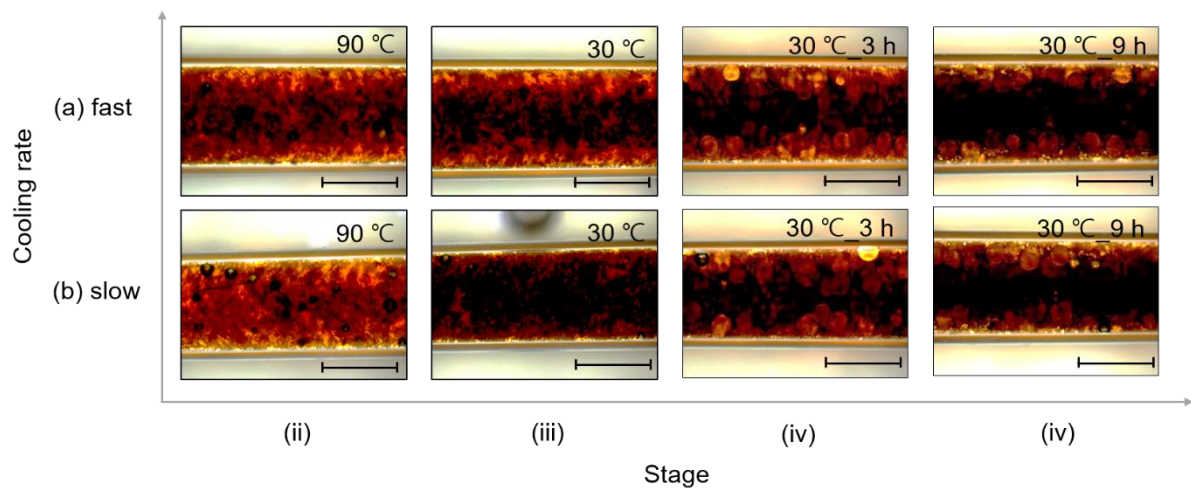


Figure 4. POM images of GO LC with the polymer crystallization. The scale bars are 1 mm

In addition, we performed SAXS experiments to investigate the microstructural change of GO LC with polymer crystallization in more details. When the GO forms the LC phase in a long range, stretched 2D SAXS patterns are generally found.³⁵ When GP03 was crystallized under the fast cooling rate (GP03-fast), the 2D patterns of GP03-fast was isotropic after cooling to at 30 °C. (**Figure 5a**) In addition, two isotropic rings were developed as the polymer crystallization progresses. It implies that the degree of GO LC was affected by polymer crystallization with a non-directional growth, and thereby the orientation of GO was significantly decreased. However, highly asymmetric scattering profiles was obtained at the slow cooling rate. (**Figure 5b**) In GP03-slow, 2D SAXS patterns from 5 hr to the final state at 30 °C show more stretched patterns with higher intensity along the long axis of capillary. In addition, GP15-slow show more anisotropic pattern at 7 h 18 m than any other patterns from GP15-fast. These results imply the orientation of GO LC can be enhanced by the slow crystallization of polymer.

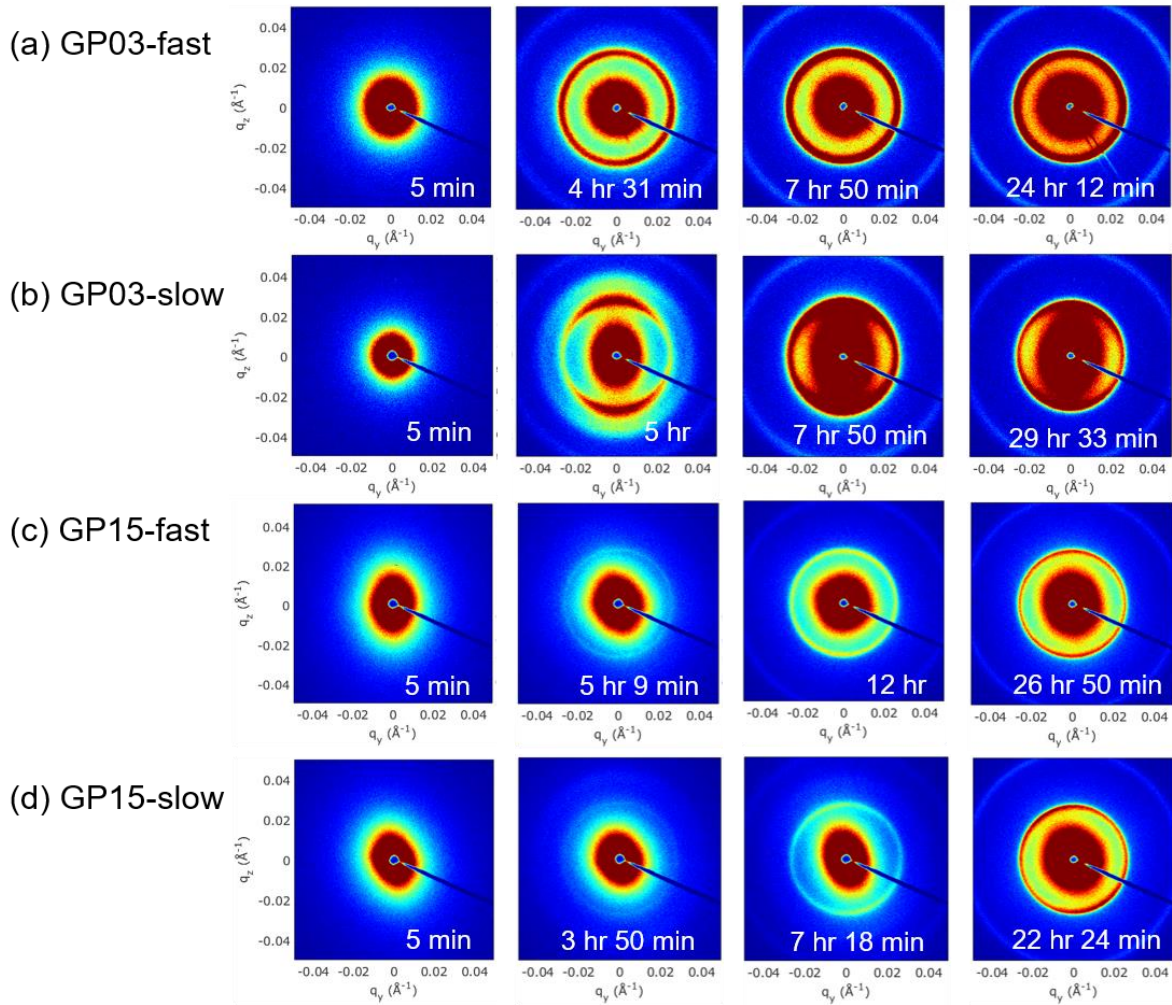


Figure 5. Selected 2D SAXS pattern of GP03 (a) and (b), GP15 (c) and (d) at different cooling rate

The effect of slow cooling rate is more pronounced at the low concentration (GP03) than at the high concentration (GP15). In GP03, more anisotropic pattern at the slow cooling rate and more isotropic patterns at the fast cooling rate were shown; huge different LC behavior of GO was shown. (**Figure 5a and 5b**) However, in the fully crystallized final state of GP15, 2D SAXS patterns show the weakly stretched patterns at both fast and slow cooling rates. (**Figure 5c and 5d**) It suggests that the decreased degree of GO LC by the PEG crystallization was similar despite the different cooling rate. At high contents of GP15, the polymer mobility/structure can be more restricted than GP03 as interdistance between GOs becomes closer. The GO contents and cooling rates competitively influence on the GO LC in semicrystalline polymer matrix.

3.1.2. Polymer Crystallization with GO LC at Controlled Cooling Rate

Then, we focused on how the addition of GO conversely affect the PEG crystallization: crystal structure and the kinetics of crystallization. **Figure 6** shows the WAXS profiles at selected times for crystallization at 5 °C/min. In **Figure 6a and 6b**, no systematic changes in the positions of the WAXS crystalline reflection were noted during the crystallization of either neat PEG or GP15 composite. There are two signature peaks located at $2\theta = 19^\circ$ and 23.3° , which arise from (021) and (032) reflections of the PEG crystals with monoclinic unit cells, respectively.³⁶⁻³⁷ It implies that the addition of GO did not affect the PEG crystal structure at atomic scales. Instead, GP15 composite shows the accelerated PEG crystallization in **Figure 6b**. The pure PEG did not show a crystal peak even after being held at 30 °C for 10 m, but the GP15 composites exhibited first crystal reflections at 32 °C before reaching 30 °C. It implies that the kinetics of polymer crystallization could be enhanced in the presence of GO. In previous research, polymer chain could easily align at the interface of GO with high specific surface areas³⁸, which reduces the nucleation barrier, and thereby the addition of GO exerts positive effect on the PEG crystallization. In addition, it was reported that strong interfacial adhesion between polymer chain with hydroxyl group and GO nanosheets exist.^{29-30, 39}

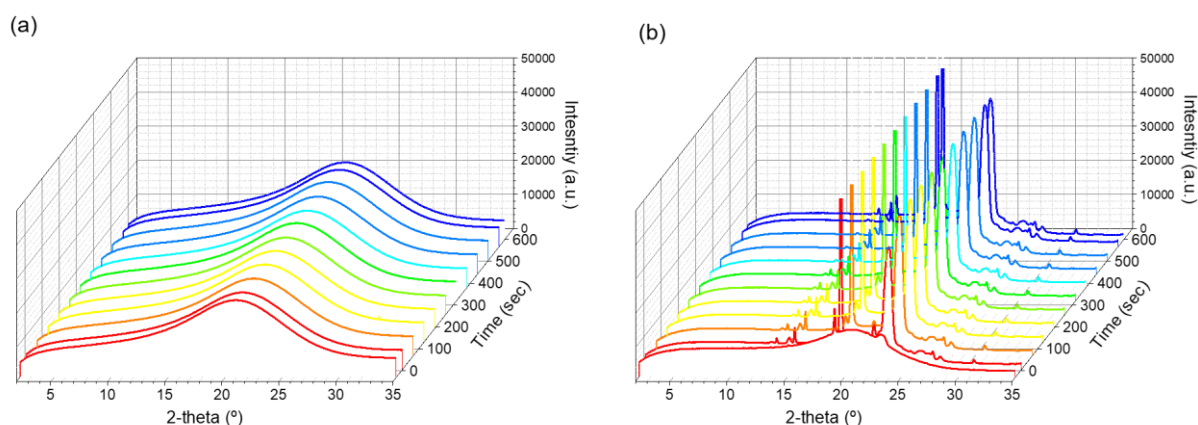


Figure 6. Development of WAXS profiles as a function of crystallization time for PEG (a) and GP15 (b)

Furthermore, the microstructural change of PEG crystals in GO suspension was investigated through the SAXS experiment. **Figure 7a and 7b** show the normalized intensity vs. q plot of GP03-fast and slow at the selected crystallization time, respectively. They show the development of crystal peaks from PEG lamellae structure. After 30 m, PEG in GP03-fast (**Figure 7a**), exhibits the high peak at the scattering vector $q = 0.04 \text{ \AA}^{-1}$ and the low peak at $q = 0.08 \text{ \AA}^{-1}$ which are the first and the second diffraction peaks. The corresponding long period L_0 of PEG lamellar stacks was about 15.77 nm calculated from Bragg's law $L_0 = 2n\pi/q$ (where n is the diffraction order and q is the scattering

vector), which indicates the twice-folded lamellar structure.⁴⁰ Further crystallization, after 7 h 50 m, PEG showed well resolved peaks at $q = 0.026, 0.052$ and 0.078 \AA^{-1} which indicate the first, second, and third orders of lamellar stacks, respectively. The corresponding long period L_0 was about 24 nm which indicates the once-folded lamellae. This peak shift phenomenon confirms the unfolding of PEG lamellae from twice-folded into once-folded structure, and the lamellar thickening behavior generally shown in low molecular weight PEG occurs regardless of cooling rate and GO concentration. (**Figure 7c and 7d**). It implies the addition of GO did not change the lamellar thickening behavior of PEG crystal.

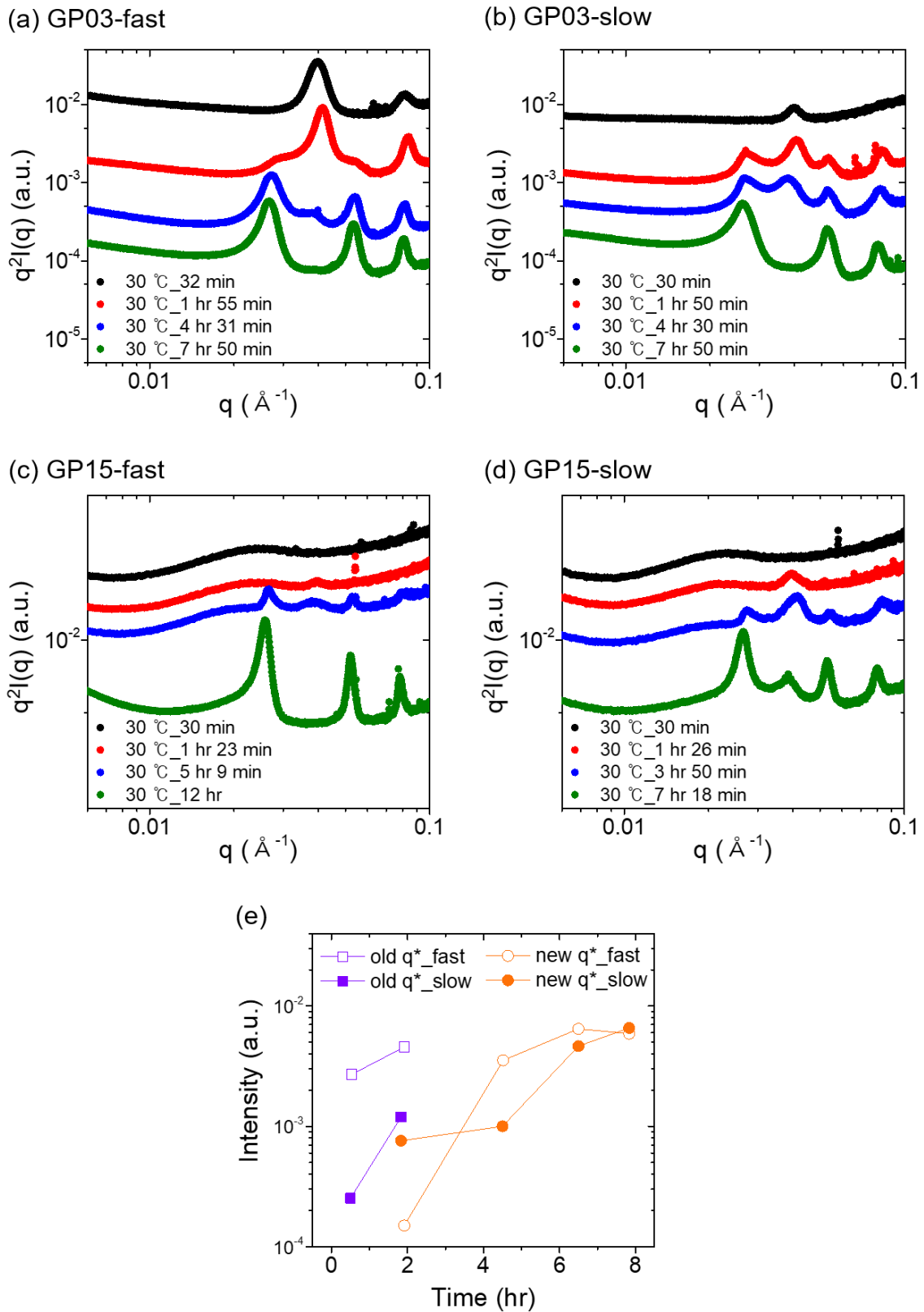


Figure 7. Kratky plots of GP03-fast (a) and slow (b), GP15-fast (c) and slow (d), and intensity of q^* versus time of GP03 (e).

However, the speed of lamellar thickening was varied depending on the cooling rate. **Figure 7e** show a growth rate of PEG crystals at fast and slow cooling rates; we extracted maximum scattering intensity at 1st crystal peak (**Figure 7a an 7b**), which indicates once-folded structure, and then compared the intensity with the holding time at 30 °C. At GP03-fast, the growth rate of peak intensity at early time was faster than GP03-slow. It means that the PEG crystallization at the fast cooling rate progress faster and show higher crystallinity. As the system approach the temperature more rapidly, more nucleation points are created simultaneously. In terms of GO LC, the rapid growth of PEG crystals could prevents GO from prepositioning in polymer matrix to form LC phase. Therefore, slower cooling rate would be preferable to GO LC because less nucleation points in polymer matrix are found. In addition, 2D SAXS pattern at GP03-slow and GP15-slow show increased anisotropy than GP03-fast and GP15-fast in **Figure 7** showing the kinetics of PEG crystallization considerably affected the GO LC.

3.1.3 Effect of Cooling Rate on GO LC with Polymer Crystallization

Moreover, we investigated the effect of cooling rate on GO LC and PEG crystal morphology. The azimuthal distribution was obtained at specific q -range, $0.004 - 0.02 \text{ \AA}^{-1}$ and $0.016 - 0.036 \text{ \AA}^{-1}$. The peaks of PEG crystal were not appeared between 0.004 and 0.02 \AA^{-1} (black symbol in **Figure 8**), and thus the structural information about GO LC would be more dominant. In contrast, at a range from 0.016 to 0.036 \AA^{-1} (red symbol in **Figure 8**), the structural information about PEG crystals would be more dominant along with structure of GO LC. In **Figure 8a**, following the crystallization during 7 h 50 m, GP03-fast shows randomly distributed curves over the azimuthal angle, which is consistent with the result of isotropic scattering pattern. (**Figure 8a**) However, GP03-slow (**Figure 8b**), which undergo the same crystallization time, exhibits a sharp peak at 90° . Importantly, the increased intensity along the long axis of capillary is attributed to PEG crystal growth in the direction guided by GOs. It indicates PEG in GO suspension prefer to crystallize on the surface of GO at the slow cooling rate. Moreover, it suggests that the directionality of GO LC could be improved when PEG develop to ordered crystal structure by the slow cooling rate.

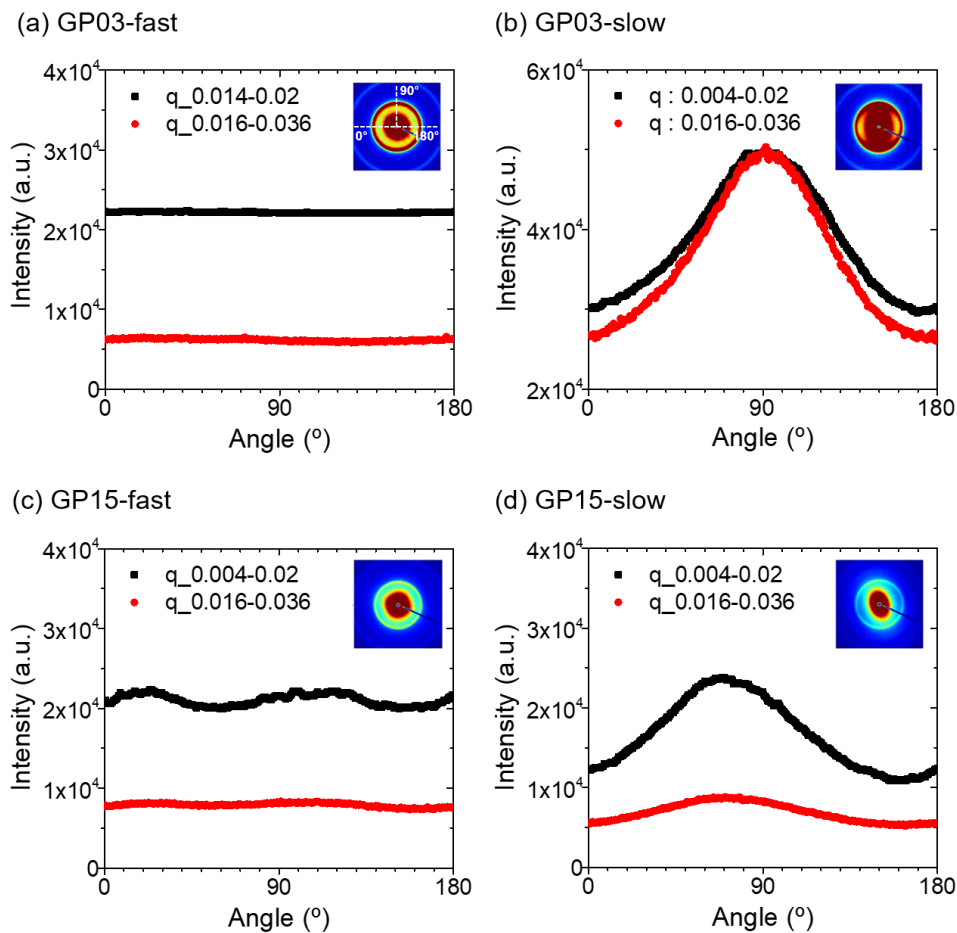


Figure 8. Angle distribution curves at GP03-fast (a) and slow (b), GP15-fast (c) and slow (d).

To quantify the macroscopic ordering of the GO LC at different cooling rate, the Hermans orientation parameter (HOF), S , is calculated which is defined as $S = (3\langle \cos^2 \theta \rangle - 1)/2$.⁴¹ (Figure 9) Here θ is the azimuth angle as shown in Figure 8a, and $\langle \cos^2 \theta \rangle = \sum_{\theta=0}^{90^\circ} I(\theta) \sin \theta \cos^2 \theta / \sum_{\theta=0}^{90^\circ} I(\theta) \sin \theta$. When S is the value of 1, -0.5 or 0, the GO sheets are perfectly aligned parallel, perpendicular or randomly to the longest axis of the capillary cells. The obtained S at the final state of GP03-fast, following whole crystallization during 24 hr, was about -0.35. It indicates that GO sheets are oriented perpendicularly to the capillary. In contrast, S at the final state of GP03-slow significantly increased up to +0.39. This confirmed that the slow and interfacial crystallization of PEG dramatically improved the GO alignment, as indicated in previous results.

Interestingly, although GP15 is higher concentration than the critical concentration where GO LC can be formed, S values from both GP15-fast and GP15-slow is smaller than that from GP03-slow. It implies that the liquid crystallinity of GP03 can be more increased than GP15 if the speed of crystallization is controlled slowly. It is meaningful to note that the cooling rate for polymer crystallization plays an important role in controlling the orientation of GO in semicrystalline polymer matrix beyond the concentration effect of GO.

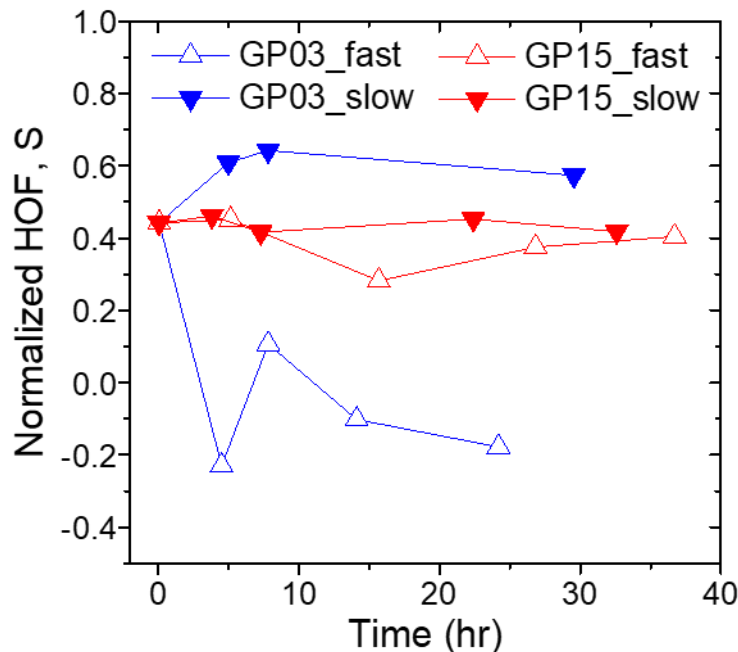


Figure 9. HOF values as a function of crystallization time.

3.1.4 Evolution of Lamellar Thickness of PEG and d-spacing of GO at Different Cooling Rate

This observation was further supported by the results of lamellar thickness and d-spacing between GO sheets at different cooling rate. **Figure 10a and 10b** show the development of q^* (1^{st} peak) from once-folded lamellae during the selected holding time at 30 °C. Interestingly, at the result of GP03 (**Figure 10a**), a lower q^* scale was shown at the slow cooling rate (filled symbol), compared to the fast cooling rate (empty symbol); the lamellar thickness of PEG was thicker at GP03-slow than GP03-fast. These results can prove that the slow cooling rate led PEG crystal to grow at the surface of GO sheets, and it ultimately increased lamellar thickness of PEG crystal. Conversely, at the fast cooling rate, PEG crystals are likely to grow in a random space of polymer matrix, and thus the size of crystal could be limited by the growth of other nearby crystals. Therefore, GO is hard to form stable LC phase at the fast cooling rate. In **Figure 10b**, the lamellar thickness change of GP15 at different cooling rate occurred in contrast to that of GP03; the thickness of PEG lamellae was thicker at the fast cooling rate. However, the thickness difference at different cooling rates was less than that of GP03 presumably due to the reduced interspacing between GOs.

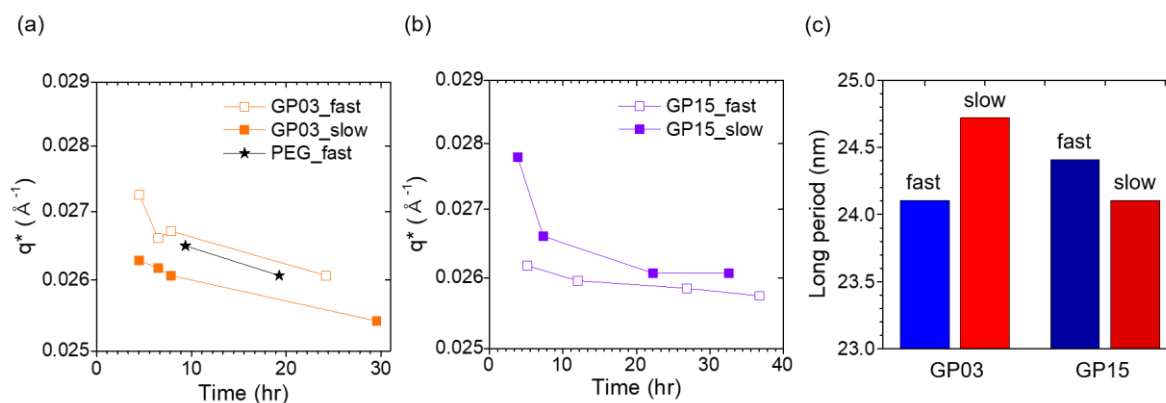


Figure 10. The value of q^* from crystal lamellae as a function of time of GP03 (a) and GP15 (b), and long period calculated at final stage (c).

Finally, we calculated the long period (L_0), the thickness of lamellar stacks, extracted from the maxima in $I(q)q^2$. (**Figure 10c**) The largest lamellar thickness was shown at GP03-slow, and the smallest lamellar thickness was shown at GP03-fast. The thicker lamellae indicate the interfacial crystallization of PEG at the surface of GO at slow cooling rate, and it could dramatically improve the orientation of both GO LC and PEG crystals. Conversely, at GP15, the lamellar thickness at GP15-fast was a bit bigger than at GP15-slow. (**Figure 10b and 10c**) Even though the PEG in GP15 was crystallized at slow cooling rate, polymer crystallization would be more restricted by confined space of highly concentrated GO. Therefore, thicker PEG crystal lamellae would be formed at GP15-fast growing crystals in less

confined region. However, the lamellae of PEG crystal in GP15-fast could not grow as largely as that in GP03-slow. It implies the interfacial crystallization occurred in GP03-slow, and the LC in GP03-slow has been positively influenced by slow crystallization. It is in good agreement with the result of the largest HOF calculation in GP03-slow. (**Figure 9**)

Moreover, we observed a change of interlayer distance between GO sheets during the polymer crystallization at the different cooling rate. **Figure 11a and 11b** show the normalized intensity plot of SAXS profiles of GP15-fast and slow, respectively. The average plane-to-plane distance, d_{avg} ($=2\pi/q^*$) could be obtained where q^* is the peak position. As the polymer crystallization proceeds further, the d_{avg} becomes larger regardless the cooling rate. (**Figure 11c**) This is due to the fact that the growing crystal of polymer would pull GO nanosheets, and thereby LC of GO was interrupted by the polymer crystallization by moving away. Interestingly, the value of d_{avg} at the slow cooling rate was larger about 2 nm than that at the fast cooling rate. We noted that the crystallization behavior at the surface of GO is more favorable at the slow cooling rate, and thereby the far distance between GO sheets was shown. The larger d_{avg} is coincidence with the swelling of lamellar thickness at the slow cooling rate in **Figure 10**.

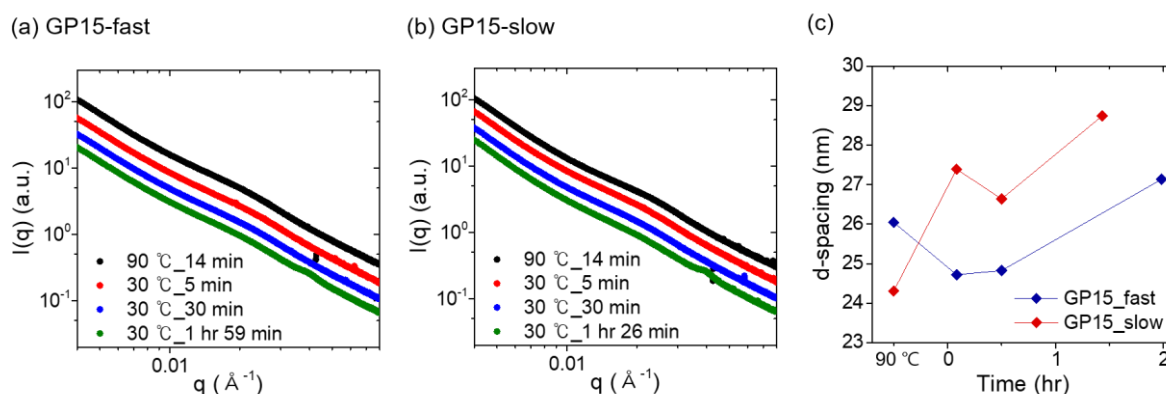


Figure 11. 1D plots of GP15-fast (a) and slow (b), and d-spacing of GO in GP15 (c).

Finally, we presented schematic images for GO LC behavior with polymer crystallization under different cooling rate and GO concentration based on our discussion. (**Figure 12**) The LC of GO was indicated by the bright yellow (increased LC) and dark brown color (decreased LC). GP03-fast show the lowest LC of GO and GP03-slow has the highest LC of GO. GO LC of GP03 was significantly affected by the cooling rate. Slow crystallization led the interfacial crystallization on the surface of GO, and thus the orientation of both GO LC and polymer crystal was increased as shown in GP03-slow and GP15-slow. The LC of GO in GP15-fast and slow was not significantly different (same colored GO sheets). However, d-spacing of GP15-fast was smaller than GP15-slow. In GP15-fast, PEG

crystallization occurs at random space and interlayer distance was decreased. At GP15-slow, interfacial crystallization at GO increased interlayer distance.

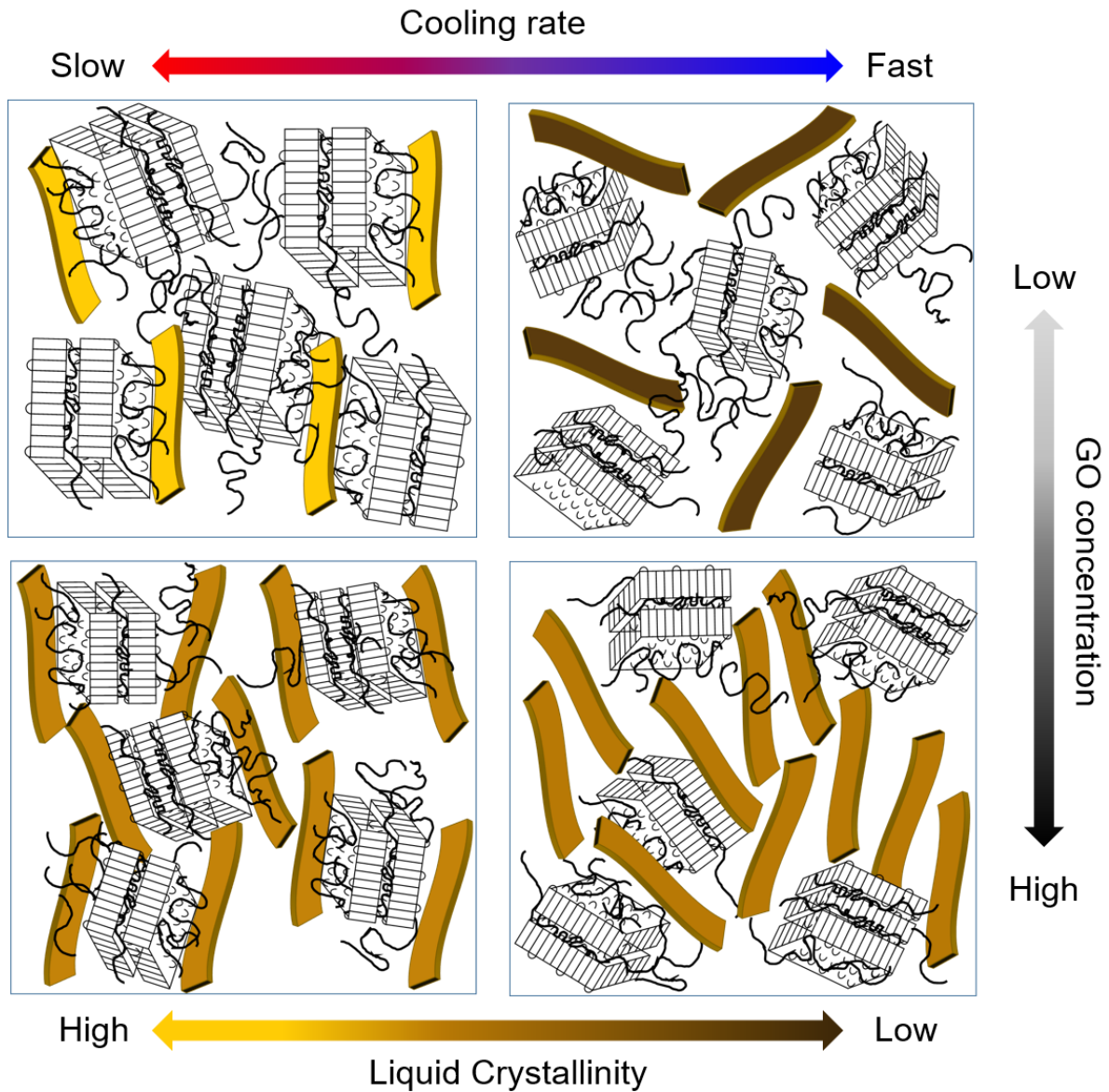


Figure 12. Schematic images of GO LC with polymer crystal structure cooling at fast and slow speed.

3.2. GO LC behavior in film system

In addition to the investigation of GO LC behavior with polymer crystallization in the bulk system, we observed the GO/PEG complex structure in film system. **Figure 13** show the optical images of GO/PEG film on the mica sheets at the different GO concentration and cooling rates. The film texture of GP03-fast and GP15-fast (**Figure 13a and 13c**) were uneven, and partial phase separation appeared. At the slow cooling rate (**Figure 13b and 13d**), the GO and PEG were homogeneously distributed with larger grain sizes, and some cracks were observed.

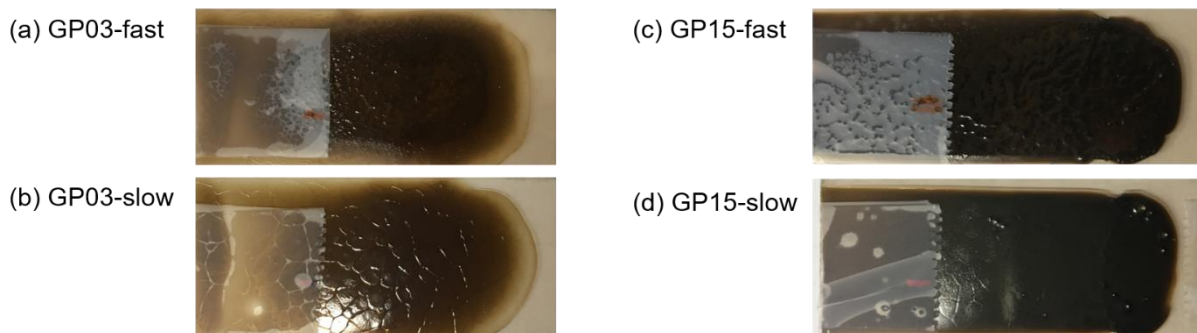


Figure 13. Real image of GO/PEG film cooling at fast and slow speed.

This observation was supported by the scanning electron microscopy (SEM) and SAXS measurement. **Figure 14a** and **14b** shows (SEM) images of GP15 film cooling at fast and slow speed, respectively. At the fast cooling rate, GO sheets were more crumpled and aggregated by polymer crystallization. (Figure 14a) In contrast, at the slow cooling rate, highly aligned GO sheets was observed without polymer crystals, and GP15-slow are aligned along the casting direction (**Figure 14b**). Thus, if we controlled the cooling rate, we can also control the GO LC in the film system.

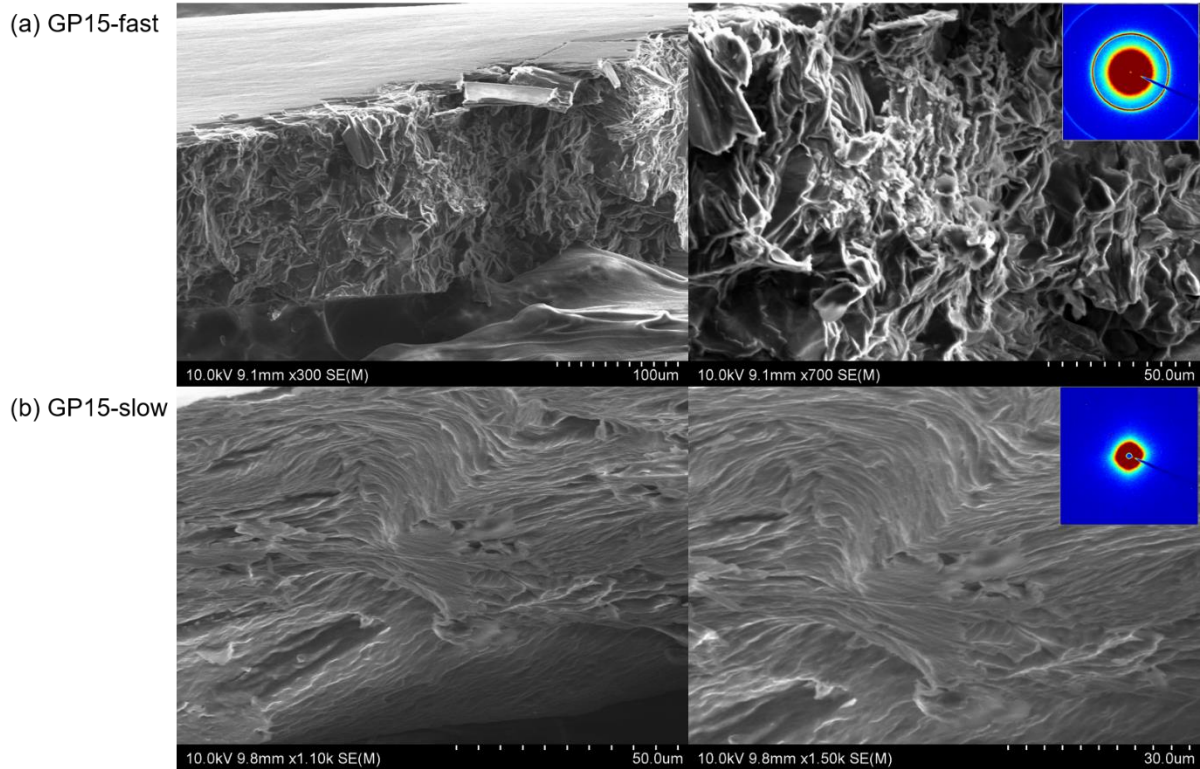
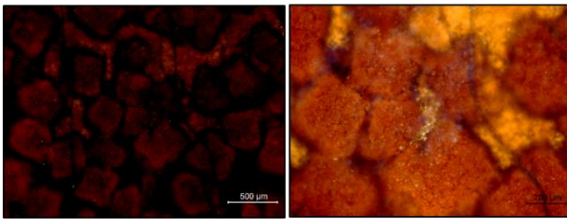


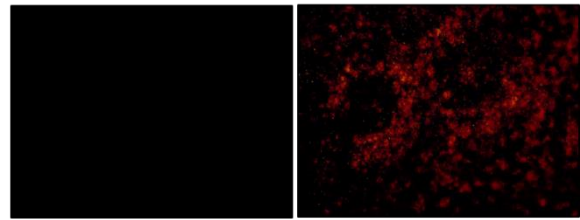
Figure 14. SEM images of cross-section of GP15-fast (a) and slow (b) film and the inset image show SAXS 2D patterns of films.

Figure 15a-b and 15c-d show POM images of GP03 and GP15 film, respectively, cooling at fast and slow rates. From the LC of GO, the brightness of birefringence of GO was higher at GP03-slow than at GP03-fast. In addition, GO LC at slow cooling rate was formed with larger domain compared to fast cooling rate. Conversely, GO LC at GP03-fast show the dark images in POM results, and smaller domain with aggregated stacks consisting of GO LC and PEG crystals was shown. The different structure from different cooling rates suggest that GO LC behavior and PEG crystallization would be competitive depending on the cooling rate, and finally GO LC behavior takes an advantage than the polymer crystallization at slow cooling rate.

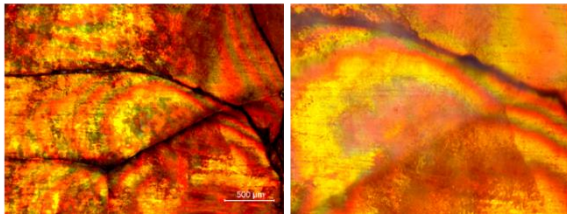
(a) GP03-fast



(c) GP15-fast



(b) GP03-slow



(d) GP15-slow

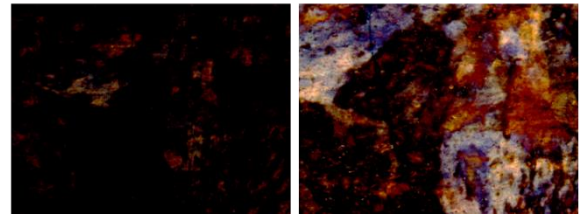


Figure 15. POM images of GO LC with PEG.

IV. Conclusion

4.1. GO LC behavior in bulk system

We have thoroughly investigated the effect of cooling rate and polymer crystallization on the microstructure of GO LC through time-resolved observation during the crystallization. Definitely, there is a correlation between microstructure of GO LC and polymer crystal structure. Moreover, their structure was affected by fast and slow cooling rate. At the slow cooling rate, PEG crystallized favorably at the surface of GO sheets, and thus the orientation of both LC of GO and PEG crystal was improved. The effect of cooling rate on GO LC was more pronounced at the lower concentration (0.3 wt%) than the higher concentration (1.5 wt%), which means that the cooling rate effect can be more important than the concentration for the GO LC in semicrystalline polymer matrix. In conclusion, based on the understanding of the correlation between the microstructure of GO LC and the crystal structure of polymer, we suggested the possibility to control the orientation of GO LC with polymer crystallization by the different cooling rate.

4.2. GO LC behavior in film system

In film system, PEG crystal structure was dominant at the fast cooling rate, and GO LC was dominant structure at the slow cooling rate. In POM observation, at GP03-fast, the complex structure consisting of GO LC and spherulite of polymer crystals. This observation was supported by SEM and SAXS measurement. At the fast cooling rate, GO sheets were more crumpled and aggregated by polymer crystallization. In contrast, at the slow cooling rate, highly aligned GO sheets was observed without polymer crystals. Thus, if we controlled the cooling rate, we can also control the liquid crystallinity of GO in the film system.

References

1. Novoselov, K. S.; Geim, A. K.; Morozov, S. V.; Jiang, D.; Zhang, Y.; Dubonos, S. V.; Grigorieva, I. V.; Firsov, A. A., Electric field effect in atomically thin carbon films. *science* **2004**, *306* (5696), 666-669.
2. Allen, M. J.; Tung, V. C.; Kaner, R. B., Honeycomb carbon: a review of graphene. *Chemical reviews* **2009**, *110* (1), 132-145.
3. Kim, K. S.; Zhao, Y.; Jang, H.; Lee, S. Y.; Kim, J. M.; Kim, K. S.; Ahn, J.-H.; Kim, P.; Choi, J.-Y.; Hong, B. H., Large-scale pattern growth of graphene films for stretchable transparent electrodes. *nature* **2009**, *457* (7230), 706.
4. Wu, D.; Zhang, F.; Liang, H.; Feng, X., Nanocomposites and macroscopic materials: assembly of chemically modified graphene sheets. *Chemical Society Reviews* **2012**, *41* (18), 6160-6177.
5. Xu, M.; Liang, T.; Shi, M.; Chen, H., Graphene-like two-dimensional materials. *Chemical reviews* **2013**, *113* (5), 3766-3798.
6. Das, S.; Robinson, J. A.; Dubey, M.; Terrones, H.; Terrones, M., Beyond graphene: progress in novel two-dimensional materials and van der Waals solids. *Annual Review of Materials Research* **2015**, *45*, 1-27.
7. Zhang, Y.-L.; Chen, Q.-D.; Jin, Z.; Kim, E.; Sun, H.-B., Biomimetic graphene films and their properties. *Nanoscale* **2012**, *4* (16), 4858-4869.
8. Scarselli, M.; Castrucci, P.; De Crescenzi, M., Electronic and optoelectronic nano-devices based on carbon nanotubes. *Journal of Physics: Condensed Matter* **2012**, *24* (31), 313202.
9. Narayan, R.; Kim, J. E.; Kim, J. Y.; Lee, K. E.; Kim, S. O., Graphene oxide liquid crystals: discovery, evolution and applications. *Advanced Materials* **2016**, *28* (16), 3045-3068.
10. Brodie, B. C., XIII. On the atomic weight of graphite. *Philosophical Transactions of the Royal Society of London* **1859**, (149), 249-259.
11. Park, S.; Ruoff, R. S., Chemical methods for the production of graphenes. *Nature nanotechnology* **2009**, *4* (4), 217.
12. Xu, Y.; Bai, H.; Lu, G.; Li, C.; Shi, G., Flexible graphene films via the filtration of water-soluble noncovalent functionalized graphene sheets. *Journal of the American Chemical Society* **2008**, *130* (18), 5856-5857.
13. Stankovich, S.; Dikin, D. A.; Dommett, G. H.; Kohlhaas, K. M.; Zimney, E. J.; Stach, E. A.; Piner, R. D.; Nguyen, S. T.; Ruoff, R. S., Graphene-based composite materials. *nature* **2006**, *442* (7100), 282.
14. Qi, X.; Pu, K. Y.; Li, H.; Zhou, X.; Wu, S.; Fan, Q. L.; Liu, B.; Boey, F.; Huang, W.; Zhang, H., Amphiphilic graphene composites. *Angewandte Chemie International Edition* **2010**, *49* (49),

9426-9429.

15. Qi, X.; Pu, K. Y.; Zhou, X.; Li, H.; Liu, B.; Boey, F.; Huang, W.; Zhang, H., Conjugated-polyelectrolyte-functionalized reduced graphene oxide with excellent solubility and stability in polar solvents. *Small* **2010**, *6* (5), 663-669.
16. Huang, X.; Qi, X.; Boey, F.; Zhang, H., Graphene-based composites. *Chemical Society Reviews* **2012**, *41* (2), 666-686.
17. Yang, X.; Zhang, X.; Ma, Y.; Huang, Y.; Wang, Y.; Chen, Y., Superparamagnetic graphene oxide-Fe₃O₄ nanoparticles hybrid for controlled targeted drug carriers. *Journal of materials chemistry* **2009**, *19* (18), 2710-2714.
18. Cao, X.; Zheng, B.; Rui, X.; Shi, W.; Yan, Q.; Zhang, H., Metal oxide-coated three-dimensional graphene prepared by the use of metal-organic frameworks as precursors. *Angewandte chemie international edition* **2014**, *53* (5), 1404-1409.
19. Huang, X.; Li, S.; Huang, Y.; Wu, S.; Zhou, X.; Li, S.; Gan, C. L.; Boey, F.; Mirkin, C. A.; Zhang, H., Synthesis of hexagonal close-packed gold nanostructures. *Nature communications* **2011**, *2*, 292.
20. Huang, X.; Zhou, X.; Wu, S.; Wei, Y.; Qi, X.; Zhang, J.; Boey, F.; Zhang, H., Reduced graphene oxide-templated photochemical synthesis and in situ assembly of Au nanodots to orderly patterned Au nanodot chains. *Small* **2010**, *6* (4), 513-516.
21. Huang, X.; Yin, Z.; Wu, S.; Qi, X.; He, Q.; Zhang, Q.; Yan, Q.; Boey, F.; Zhang, H., Graphene-based materials: synthesis, characterization, properties, and applications. *small* **2011**, *7* (14), 1876-1902.
22. Marcano, D. C.; Kosynkin, D. V.; Berlin, J. M.; Sinitskii, A.; Sun, Z.; Slesarev, A.; Alemany, L. B.; Lu, W.; Tour, J. M., Improved synthesis of graphene oxide. *ACS nano* **2010**, *4* (8), 4806-4814.
23. Donald, A. M.; Windle, A. H.; Hanna, S., *Liquid crystalline polymers*. Cambridge University Press: 2006.
24. Xu, Z.; Gao, C., Graphene chiral liquid crystals and macroscopic assembled fibres. *Nature communications* **2011**, *2*, 571.
25. Jalili, R.; Aboutalebi, S. H.; Esrafilzadeh, D.; Konstantinov, K.; Moulton, S. E.; Razal, J. M.; Wallace, G. G., Organic solvent-based graphene oxide liquid crystals: a facile route toward the next generation of self-assembled layer-by-layer multifunctional 3D architectures. *Acs Nano* **2013**, *7* (5), 3981-3990.
26. Xu, Z.; Gao, C., Aqueous liquid crystals of graphene oxide. *Acs Nano* **2011**, *5* (4), 2908-2915.
27. Cheng, C.; Li, D., Solvated graphenes: an emerging class of functional soft materials. *Advanced Materials* **2013**, *25* (1), 13-30.

28. Dikin, D. A.; Stankovich, S.; Zimney, E. J.; Piner, R. D.; Dommett, G. H.; Evmenenko, G.; Nguyen, S. T.; Ruoff, R. S., Preparation and characterization of graphene oxide paper. *Nature* **2007**, *448* (7152), 457.
29. Xu, J.-Z.; Chen, C.; Wang, Y.; Tang, H.; Li, Z.-M.; Hsiao, B. S., Graphene nanosheets and shear flow induced crystallization in isotactic polypropylene nanocomposites. *Macromolecules* **2011**, *44* (8), 2808-2818.
30. Xu, J.-Z.; Liang, Y.-Y.; Zhong, G.-J.; Li, H.-L.; Chen, C.; Li, L.-B.; Li, Z.-M., Graphene oxide nanosheet induced intrachain conformational ordering in a semicrystalline polymer. *The journal of physical chemistry letters* **2012**, *3* (4), 530-535.
31. Kim, S. J.; Kim, D. W.; Cho, K. M.; Kang, K. M.; Choi, J.; Kim, D.; Jung, H.-T., Ultrathin graphene oxide membranes on freestanding carbon nanotube supports for enhanced selective permeation in organic solvents. *Scientific reports* **2018**, *8* (1), 1959.
32. Godfrin, M. P.; Guo, F.; Chakraborty, I.; Heeder, N.; Shukla, A.; Bose, A.; Hurt, R. H.; Tripathi, A., Shear-directed assembly of graphene oxide in aqueous dispersions into ordered arrays. *Langmuir* **2013**, *29* (43), 13162-13167.
33. Kim, J. E.; Han, T. H.; Lee, S. H.; Kim, J. Y.; Ahn, C. W.; Yun, J. M.; Kim, S. O., Graphene oxide liquid crystals. *Angewandte Chemie International Edition* **2011**, *50* (13), 3043-3047.
34. Kumar, P.; Maiti, U. N.; Lee, K. E.; Kim, S. O., Rheological properties of graphene oxide liquid crystal. *Carbon* **2014**, *80*, 453-461.
35. Callies, X.; Véchambre, C.; Fonteneau, C.; Pensec, S.; Chenal, J.-M.; Chazeau, L.; Bouteiller, L.; Ducouret, G.; Creton, C., Linear rheology of supramolecular polymers center-functionalized with strong stickers. *Macromolecules* **2015**, *48* (19), 7320-7326.
36. Pulst, M.; Samiullah, M. H.; Baumeister, U.; Prehm, M.; Balko, J.; Thurn-Albrecht, T.; Busse, K.; Golitsyn, Y.; Reichert, D.; Kressler, J. r., Crystallization of Poly (ethylene oxide) with a Well-Defined Point Defect in the Middle of the Polymer Chain. *Macromolecules* **2016**, *49* (17), 6609-6620.
37. Lisowski, M. S.; Liu, Q.; Cho, J.; Runt, J.; Yeh, F.; Hsiao, B. S., Crystallization behavior of poly (ethylene oxide) and its blends using time-resolved wide-and small-angle X-ray scattering. *Macromolecules* **2000**, *33* (13), 4842-4849.
38. Grady, B. P.; Pompeo, F.; Shambaugh, R. L.; Resasco, D. E., Nucleation of polypropylene crystallization by single-walled carbon nanotubes. *The Journal of Physical Chemistry B* **2002**, *106* (23), 5852-5858.
39. Huang, H.-D.; Xu, J.-Z.; Fan, Y.; Xu, L.; Li, Z.-M., Poly (L-lactic acid) crystallization in a confined space containing graphene oxide nanosheets. *The Journal of Physical Chemistry B* **2013**, *117* (36), 10641-10651.

40. Van Duong, T.; Goderis, B.; Van Humbeeck, J.; Van den Mooter, G., Microstructure of pharmaceutical semicrystalline dispersions: the significance of polymer conformation. *Molecular pharmaceutics* **2018**, *15* (2), 629-641.
41. Prost, J., *The physics of liquid crystals*. Oxford university press: 1995; Vol. 83.